Monitoring Pollutant Emission with QC Laser Based Mid IR Sensors

Ferdinand Shimei. I. [a*], Chineke, T. C. [b], Nwofor, O. K. [c], Ewurum, B. B. [d]

[a,b,c,d] Department of Physics and Industrial Physics, Imo State University, P.M.B 2000 Owerri, Nigeria

[a] Email: jehos_haphat@yahoo.com

Abstract

Current progress in Mid-IR semiconductor laser technology established on inter-sub-band changed like quantum wells assure a remarkable impact on tunable diode laser-based sensors for trace gases. This paper presents improvement toward the awareness of room-temperature laser-based sensors for combustion-generated pollutants like NO_2 and SO_2. Laboratory measurements of SO_2 at 8.5 µm are presented with detection range on the order of 1 ppm. Further approaches for higher sensitivity measurements in exhaust gas conditions are illustrated, as well as measurements of SO_x.

Keywords: Pollutant- Combustion- Sensors; Quantum –Cascade; Diode- Laser.

1. Introduction

Contemporary jet aircraft engines generate oxidized sulfur type, such as SO_2, SO_3, and H_2SO_4, which may contribute to the formation of aerosols and clouds in the atmosphere [1]. The reaction mechanisms and rates for conversion of combustion-generated SO_2 to SO_3 and next to H_2SO_4 in jet aircraft exhausts are the subjects of severe inspection in the assessment of the atmospheric effects of aviation, which can be determined by quantitative determinations of SO_2 and SO_3 yields in the exhaust streams of test engines at high-altitude speed atmosphere. Fuel-bound sulfur is currently in jet fuels as pollution and as lubricant agents. For the period of the combustion process in the engine, this sulfur is fundamentally completely corroded to structure SO_2, which is exhausted into the atmosphere.

----

* Corresponding author

Some of the SO_2 further corroded over a long time scale by atmospheric order to form H_2SO_4, which condenses to form tiny aerosol particles. Furthermore, some of the SO_2 is rapidly corroded in combustor exhaust stream to generate SO_3, which is in turn rapidly transformed into H_2SO_4 through result with H_2O in the exhaust. However, [2, 3] elaborated further how H_2SO_4 formed in the exhaust stream may deposit on combustion-generated soot particles to produce hydrophilic condensation nuclei, thereby promoting formation of contrails and unrelenting cirrus clouds in the stir of the aircraft. These clouds and their development in highly traveled aircraft passageway can have significant impacts on the radiate heat and chill budgets in the local upper troposphere and lower stratosphere, with extremely uncertain effects on area climate and on mass shift across the tropopause [1]. Thus aircraft-generated high-altitude clouds, resulting from SOx chemistry in the exhaust, may affect global climate and stratospheric ozone dynamics.

Due to potentially severe long-term atmospheric effects, governments and industrial research and development of complex gas turbine engine model are pursuing means of confirming and quantifying the linkages between fuel-bound sulfur, combustion-generated SO_2, SO_3, and H_2SO_4, and the formation of condensation nuclei. Key factor of this research and development is the determination of the kinetics, concentrations, and chemical fates of SO_2 and SO_3 in combustor exhaust streams. It call for highly sensitive (ppmv level) and quantitative detection of SO_2 and SO_3 at high temperatures (2800 to 6990 K), reduced pressures (0.2 to 0.4 atm), and elevated H_2O and CO_2 mole fractions (0.10 to 0.15) characteristic of combustor exhaust conditions. Summary of the temperature and pressure account through the exhaust turbine and the resultant equilibrium SOx concentration account is shown in Figure 1. Note that thermodynamic equilibrium favors SO_3 structure; however it is well recognized that almost all of the emitted sulfur is in the form of SO_2 due to the slow kinetic rate of conversion of SO_2 to SO_3 under these circumstances
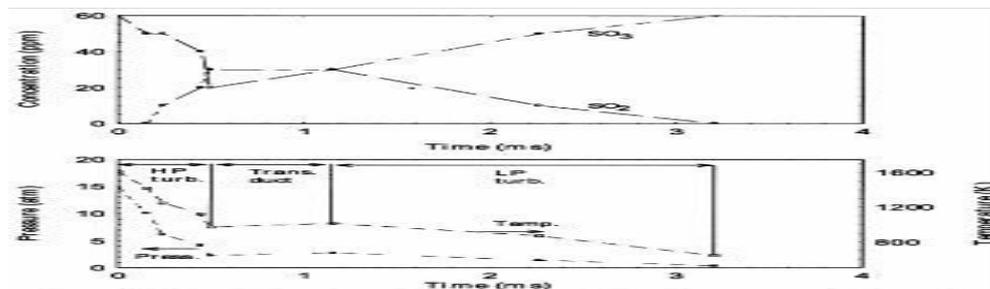
Figure 1: shows the calculated equilibrium SO_2 from a P-T cycles analysis of a commercial service jet aircraft engine operating with Jet – A fuel having 0.5% sulfur contents and at an overall equivalence ratio of 0.37.(Courtesy Dr. Quang-Viet Nguyen NASA/GRC, May 2000)

1.1 Definition of Problem

The increase in anthropogenic activities from jet aircraft exhaust increased the level of pollution in atmosphere as particulate matter were ejected into the atmosphere in form of fumes from the exhaust of jet aircraft engine through the exhaust. This study intends to assess room-temperature laser-based sensors for combustion-generated pollutants such as NOx and SOx.

1.2 Objectives of Study

The purpose of this study is to identify and quantifying the linkages between fuel-bound sulfur, combustion-generated SO_2, SO_3, and H_2SO_4, and the formation of condensation nuclei.

1.3 Significance of the Study

This study if properly carried out will

- Provide insight to the pollution level in atmosphere.
- Create public awareness and information to the dangers caused by pollution jet aircraft engines.
- Create better quality life and public safety health for the people if air quality of the environment is monitored.
- Reduce sickness arising from short and long term exposure to air pollution.

1.4 Limitation of Study

The limitations of this study include the following: (a) the complexity in ascertaining exact rates for conversion of combustion-generated SO_2 to SO_3 and next to H_2SO_4 in jet aircraft exhaust.

2. Review of Related Literature

2.1 SO_x Monitoring Techniques

Although procedure to detect these species have been formulated in several research laboratories, their implementation requires considerable exertion and specialized dexterity in physical chemistry, optics, and spectroscopy, so these methods are not readily available to the combustion engineering community. We observed that investigating the kinetics of SO_2 and SO_3 has devised means of detecting these species using electronic evolution in the ultraviolet area of the spectrum [4]. SO_2 can be detected by absorption or laser-induced fluorescence in its electronic bands near 298 nm. Furthermore, SO_3 has absorption bands in the vacuum ultraviolet (145 to 160 nm), and has been detected by laser photo dissociation to excite fluorescence from excited SO_2 near 298 nm. Detection of SO_3 by this method requires a fluorine excimer laser at about 157 nm, and is unworkable in systems containing substantial concentrations of oxygen since O_2 absorbs strongly at the wavelengths required to photo dissociate the SO_3. The SO_2 electronic band is accessible to pulsed tunable dye lasers, and can also be reached by frequency summing of two high-power near-IR solid state lasers in a non-linear optical crystal.

Infrared fraction of the spectrum present an alternative approach for probing trace-level gas-phase species, mostly by laser absorption in fundamental and overtone vibration-rotation bands. Nevertheless, the infrared absorption approach has in history found less application at high sensitivities than ultraviolet method owing to inherent sensitivity limitations of conventional absorption measurements and to the rareness of tolerable infrared light sources.

More than 15 years, semiconductor laser absorption spectrometers with the utmost sensitivities have operated primarily in the mid-infrared, where the fundamental vibration evolution occurs. These evolutions have the largest infrared evolution strengths for a given molecule, while they arise from single-quantum change in the vibration quantum number. Accordingly they accessed this wavelength region, laser absorption spectrometers have been developed using lead salt diode lasers [5]. Although these devices have achieved high sensitivities and have operated on airplanes, balloons, and combustion facilities, there are several aspects of lead salt lasers that result in a complex instrument design or inhibit routine use. Lead salt lasers are hygroscopic, are highly sensitive to electrostatic discharge, exhibit performance degradation due to temperature cycling, and produce relatively low output power (0.1 to 1 mW). Remarkably, these lasers do not operate at room temperature but require cryogenic cooling. In addition, these lasers are only available in Fabry-Perot designs, with the result that they operate multimode and can require a monochromator to select a single longitudinal mode. They are available in few wavelengths from limited purveyor because of low demand. They found their best use in highly specialized, deep research applications.

2.2 Quantum Cascade Lasers

However, recent development of quantum cascade lasers enables the following major progression in trace type detection: entrance to the strong, mid-infrared fundamental vibration-rotation evolution with a room temperature, single-mode, tunable diode laser [6, 7]. QC lasers realize gain via the transitions of electrons between two sub bands in the conduction band of a coupled quantum well structure. Inversion is created by engineering the lifetimes of the states concerned. The paired electron-injection and active-well regions are replicated many times over (cascaded) to increase output power. Since the evolution occur completely within the conduction band of the material, the output wavelength is determined by the thickness of the active region and is independent of the band gap. QC lasers can be fabricated at any wavelength from ~ 4.6 to 17 μm using AlInAs/InGaAs lattices. The QC laser design overcomes two main drawbacks of lead salt diode lasers. First, they can be operated at room temperature, and second, depressed response (DRP) versions can be fabricated to operate on a single longitudinal mode. By accessing the stronger bands in the mid-infrared fingerprint region, a QC laser absorption spectrometer requires a considerably shorter path than a near-IR device of comparable sensitivity. These advantages result in an overall sensor system that will be smaller and less complex than existing lead salt or near-IR sensors. Thus, the advent of QC lasers enables a new generation of laser-based sensors which achieve the sensitivities of lead salt laser sensors and incorporate the robustness and ease of operation of near-IR diode laser sensors.

Many groups have recently delivered applications of QC lasers to trace gas sensing [8]. Sensitive absorption spectroscopy using frequency modulation (FM) detection and a room temperature, pulsed (DRP) QC laser has been reported. Receptive absorption spectroscopy has also been demonstrated with cryogenically cooled, as [9]. The continue wave (cw) QC lasers using either FM detection or photo acoustic detection techniques [10]. Detection of isotopic composition has also been demonstrated using cryogenically cooled cw QC lasers [11].

However, works has focused on quasi-cw, room temperature operation of the laser source with high sensitivity detection achieved using the balanced ratio metric technique [12].

They established the operation of a breadboard QC laser system to detect N_2O and NO near 5.4 μm, and are currently developing a field sensor for measurements of formaldehyde in the troposphere. Their general approach is to combine QC laser light sources with multipass absorption cell and noise reduction techniques formerly developed for our near-IR diode laser sensors, to achieve sub-ppmv sensitivities for infrared-active species. While QC lasers can be operated cw at cryogenic conditions, they took the approach of pulsed operation at thermoelectrically cooled conditions near room temperature. The noise reduction techniques include [13]:

➢ Reduction of thermal noise through use of liquid-nitrogen-cooled field of view.

➢ Dual-beam, unbiased share metric detection (USD). The USD system is an analog circuit which ratios the signal and reference beams to cancel common mode laser intensity fluctuations. Here the USD is interfaced with the pulsed laser source by operating the USD circuit at a bandwidth which is low adequate to standard the laser pulses into a "quasi-cw" sign, but high sufficient to reject common mode laser noise.

3. Methodology

3.1 IR Spectroscopy of SO_2 and SO_3

We examined the quantitative infrared spectroscopy of SO_2 and SO_3 via data bases existing in the literature. A detailed, line-by-line compilation of the vibration-rotation transitions of SO_2 is given in the HITRAN96 data base on atmospheric infrared transitions. The HITRAN cipher and data base was urbanized by the Air Force Research Laboratory to provide model simulation capability for high-resolution infrared absorption spectra of atmospheric species as functions of temperature, pressure, concentration, and path length. We also performed spectral modeling simulations using the commercial version of HITRAN marketed by Ontar Corp. The modeling calculations simulated the conditions of our room-temperature FTIR and QC laser measurements, as well as the conditions of high-temperature combustor exhaust measurements at both atmospheric and reduced pressures. The high-temperature calculations also included simulations of the absorption spectra of H_2O and CO_2, which are the most important sources of spectral interference with SO_2 and SO_3 detection in combustor exhaust streams. The high-temperature simulations of H_2O and CO_2 absorption spectra used the HITEMP spectroscopic data base for these species; this data base includes hot-band transitions which are applicable to high-temperature systems up to ~ 1000 K. Unfortunately, there is no high-temperature analogue of this data base for SO_2, so the scaling of SO_2 transitions and line strengths to combustor exhaust temperatures is not well validated.

The experimental SO_2 spectra were obtained at room temperature with a commercial FTIR spectrometer (Midac Corp.) interfaced to a multipass absorption cell. The cell was connected to a gas supply manifold and a vacuum system allowing operation from vacuum to 1 atm. The multipass optical system within the cell was set up to give 20 passes, resulting in a total path length of 4.90 m. Matched pairs of background (cell evacuated) and sample (cell containing gas sample) spectra -1 were obtained at 0.5 cm spectral resolution by co-adding 33 interferograms for each case.

The background and sample: (a) Spectra were ratio to give quantitative spectra of absorbance, in (Io/I), versus evolution frequency in cm. (b) The measurements were performed over the pressure range 0.1 to 0.4 atm for a commercial gas mixture of 502.5 ppmv SO_2 diluted in N_2.

As demonstrated by the experimental spectra in Figure2: shows SO_2 has two vibration bands in the 6 to 9 µm region: (a) the strong asymmetric stretch ($\upsilon3$) band centered near 1359 cm (7.35 µm).

(b) The weaker symmetric stretch band ($\upsilon1$) centered near -1050 cm (8.7 µm).

The 8.6 µm QC laser measurements carried out for this exertion probe the latter, $\upsilon1$ band; though, evolution in the $\upsilon3$ band will achieve the highest possible sensitivity. The most recently reported integrated band intensities at 295 K (including hot band contributions) are 0.39×10^{-17} and 2.98×10^{-17} cm/ (molecule cm^{-2}) for the $\upsilon1$ and $\upsilon3$ bands, respectively.
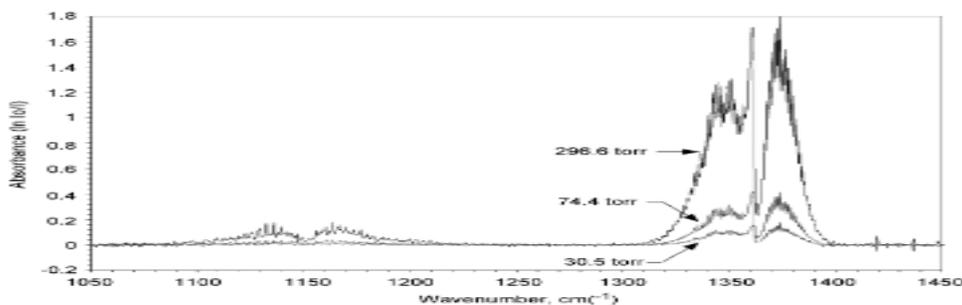
Figure 2: FTIR spectra of 502 ppm SO_2, balance N_2 at 295 K in a 4.89m path (Courtesy atmos.)

Figure 3 shows the result absorbance spectrum to check for spectral interferences by air at room temperature, we filled the FTIR absorption cell to atmospheric pressure with room air at ~ 20% relative humidity, overlain with the SO_2 spectrum. All the evolutions in the room air spectrum are due to H_2O, as confirmed by HITRAN calculations. At room temperature, there are no interfering H_2O transitions in the SO_2 ($\upsilon1$) band, confirming that the laboratory QC laser measurements at 8.5 µm did not require a purge flow in the beam path. Though, there are several H_2O features in the region of the SO_2 ($\upsilon3$) band, as this region is near the edge of the strong H_2O ($\upsilon2$) band centered near 6.2 µm. H_2O interference in this region is a key factor in the design of a system for high-temperature measurements, as described below.
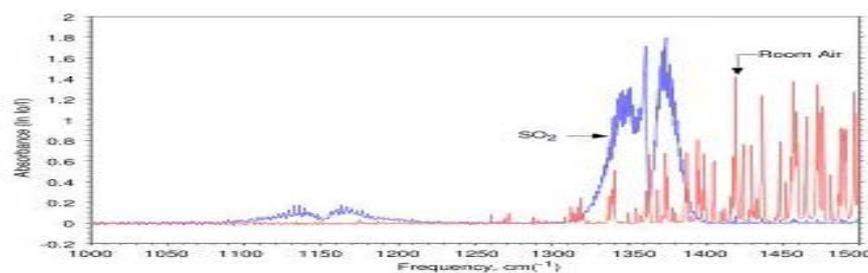
Figure 3: Comparison of FTIR spectra of SO_2 and room air, showing spectral overlap of H_2O absorption features (Courtesy Atmos.).

The infrared spectrum of gas-phase SO_3 consists of a $\upsilon3$ band centered at 1392.3 cm (7.19 µm), and $\upsilon2$ and $\upsilon4$ bending bands near 500 cm (20 µm) [14, 15]. SO_3 is a planar symmetric (D3h) molecule, and thus the symmetric stretch $\upsilon1$ is infrared-inactive. Only the $\upsilon3$ band is accessible to a QC laser. Full spectroscopic measurements of this band have been reported by Henfrey and Thrush. A section of their published spectrum, obtained at 0.01 cm^{-1} resolution for 10 Torr of SO_3 in a 15 cm gas cell, is shown in Figure 4. The authors report detailed spectroscopic constants which can be used to calculate the line-by-line transition frequencies; though no line strength data are available. The peak absorbencies shown in Figure 4 are consistent with line strengths similar in magnitude to those for SO_2 ($\upsilon3$). A broad computer literature search indicates that there are no open-literature data on the line power or high-temperature spectroscopy of this band.
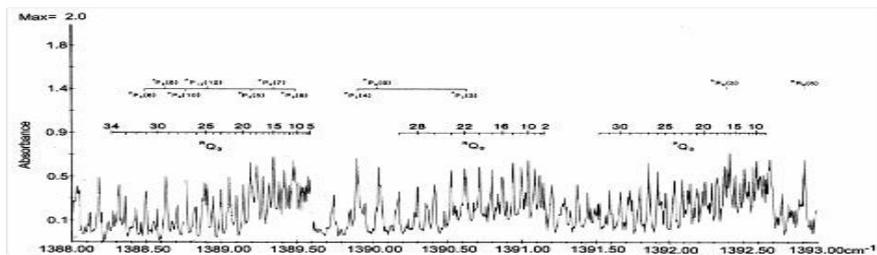
Figure 4: High resolution spectrum of the center of the SO_3 (v_3) band (Courtesy Atmos.).

4. Data Analysis

4.1 Laser Measurements on Quantum Cascade

Mutually dispersed response (DRP) and non-dispersed response (DRP) Quantum Cascade (QC) laser devices working near 8.5 µm were available to support this exertion. The dispersed response lasers of carrier D2307CC2 were partially characterized at Lucent for pulsed operation near room temperature. Figure5: is a plot of the temperature tuning for two representative QC lasers. This data was obtained for pulsed operation at 82.8 kHz with 60 ns pulse width.
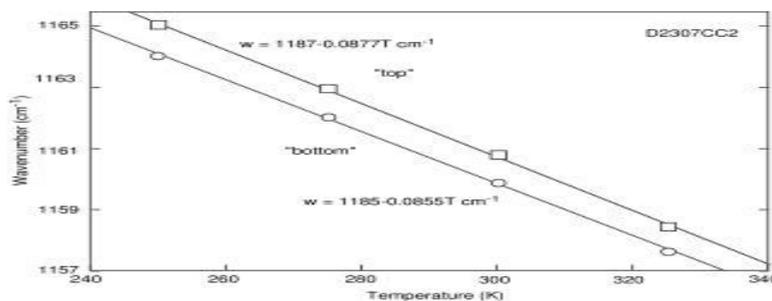
Figure 5: show Example of QC laser temperature tuning data for two devices (top and bottom) (Courtesy Atmos.)

The current tuning rate is approximately 10^{-2} cm^{-1}/mA (300 MHz/mA). Figure6: shows L-I and V-I curves presented for the laser.

These QC lasers have a current threshold of approximately 2.6 to 3.6 near room temperature and have a distinctive emission roll-off at higher currents. In between, the L-I curve is linear.
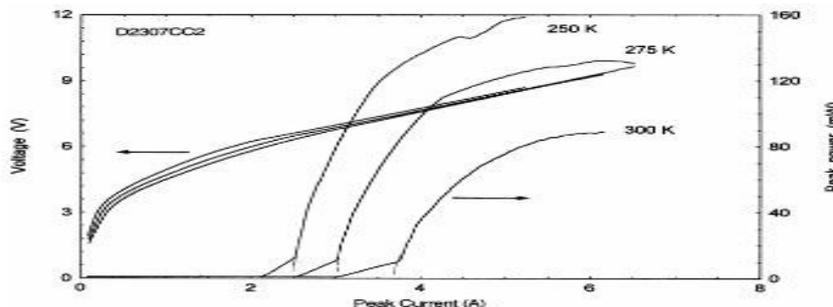
Figure 6: shows example L-1 and V-I curve for the same two devices as in figure.5. (Courtesy Atoms)

These procedures require a reasonably high compliance voltage (~5 V) compare to other semiconductor diode lasers. For zero bias, the devices have an efficient resistance of about 21 ohm, which decreases to 1.5 ohm above threshold. They described the laser system and drive current configuration for these experiments [12]. Absorption dimension were classically made by pumping the laser with a 5 kHz injection current pulse train consisting of 66 ns pulses for an overall duty cycle of 0.03%. The waveform be superimposed ahead a low-amplitude slope waveform with a typical repetition frequency of 100 Hz.

The collimated laser beam exits the mount and it split into a signal and a reference beam using an ar-coated Ge beam splitter. The signal beam propagates through a 0.5 m electro polished, stainless steel absorption cell having ar-coated, 30' wedged Ge windows. After exiting the cell, the beam is refocusing onto an LN2-cooled photovoltaic HgCdTe detector by a 1 in. diameter, ar-coated Ge f/1 lens. Similarly, the reference beam is refocused onto a second HgCdTe detector using another Ge lens. Rider was made to purge the beam paths. The detectors were 1 mm diameter devices. Each detector was fitted with a 61 deg cold field-of-view. This helps minimize the background current arising from collection of ambient radiation.

Outputs from the detectors were sent to a high gain current preamplifier then into gated integrators. The gated integrator signals were sampled, recorded and integrated to produce a real time history of the number density of the type under analysis. This dual beam, predictable detection technique allowed us to investigate spectral absorbance down to ~0.5%.

We observed the compound absorption aspect that arises from the partial overlie of six lines of the $\upsilon 1$ band that occur near 1160.76 cm (8.63 µm). These evolutions are listed in Table 1.

A forecasted absorption spectrum near 1159 cm, for 100 ppmv of SO_2 at 100 Torr, is shown in Figure 7. Further modeling with HITRAN96 at lower pressures specify that strong absorption spectra of individual transitions can be produced in the Doppler-broadened limit, using 1 to 10 Torr of undiluted SO_2 over the available 0.5 m path.

Table 1: Entity evolution in v1 Band of SO_2 causative to the Observed Absorption Features

Frequency (cm^{-1})	Line Strength (cm^{-1}(molecle^{x}cm^{-2})	Z_1			Z_2		
1161.49479	1.53 x 10^{-21}	8	3	6	6	2	6
1161. 70377	3.40 x 10^{-21}	25	5	21	**25**	**2**	**20**
1161. 77537	5.21 x 10^{-21}	16	2	16	**15**	**1**	**15**
1161. 77313	5.38 x 10^{-21}	15	1	15	16	0	16
1161. 79491	3.22 x 10^{-21}	17	2	16	16	2	17
1161. 81365	2.89 x 10^{-21}	18	2	17	17	1	16
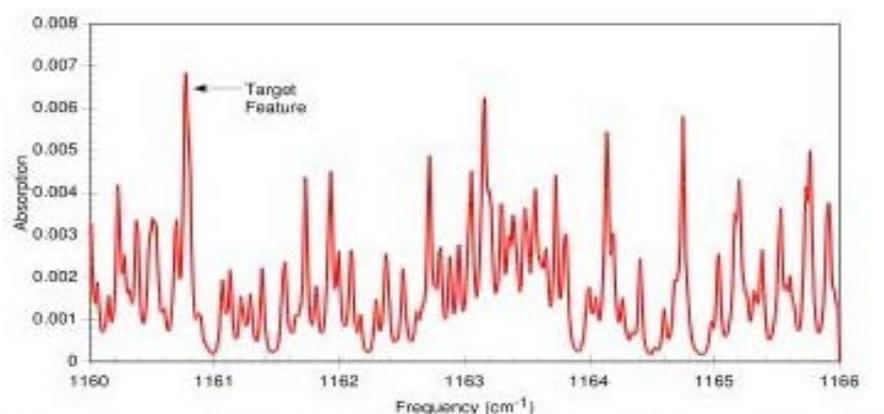
Figure 7: Computed spectrum of SO_2 absorption features near 1160 cm^{-1}, for 100ppm, SO_2/air at 100 Torr. (Courtesy Atmos.)

Certainly is important to note that the band spectrum for SO_2 is highly crammed and overlapped, even under low pressure, Doppler-broadened conditions. However, we do not sample a true zero-absorption baseline, rather the differential absorption produced by the compound, overlie features.

Model experimental absorption spectrum is existing in Figure 8. This spectrum was obtained for 0.5 Torr 16 -2 (1.6 x 10cm^{-3}) of SO_2 at 296 K, and is an average of ten single sweeps (0.1 s average). The thinner line is a running average of ten data points and advances the signal-to-noise ratio.

The peak absorption is 0.07 and the signal-to-noise ratio (SNR) is ≈30, which entail minimum detectable peak absorption of 3 x 10^{-3} for 2.6 x 10^{14} cm^{-3} SO_2 and a 1 m path. By extrapolating these results to the typical detection limits of dispersed response or FM-based spectrometers and accounting for increased collision broadening near atmospheric pressure, we approximate detection sensitivity at room temperature of about 0.1ppm
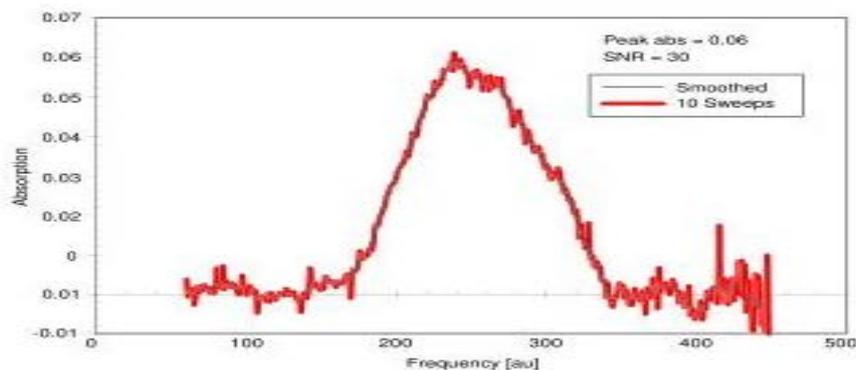
Figure 8: Examples QC laser absorption spectrum of the compound SO_2 feature near 1160.75cm^{-1}.The spectrum was obtained with 9.5 Torr SO_2 at room temperature in a 50cm cell. (Courtesy Atmos.)

4.2 Exhaust Gas Simulation Measurements

The annex of the present room-temperature results will require QC lasers working at different wavelengths so as to optimize the sensitivity of the beleaguered lines as well as ensure that they are free from interference by major exhaust gas type such as CO_2 and H_2O. In order to determine best wavelengths for SO_2 and SO_3, we used broad spectral simulations by HITRAN and HITEMP to forecast high-resolution spectral absorbance for a variety of combustion exhaust situation from 0.1 to 1 atm. A supposed set of environment used here and representative of many exhaust gas conditions in flight are P~ 0.2 atm, T~ 700 K, ΩCO_2 ~ 0.1, and ΩH_2O ~ 0.1.

The forecasted spectra were estimated in terms of absorbance per meter of path length for 1 ppmv of SO_2. In calculating the detection limits in terms of concentration and path length, we assumed a minimum detectable absorbance of 1 x 10^{-5}. They discussed this projected value based on our breadboard QC laser measurements at 5.5 and 8.5 µm with and without the DRP noise- canceling circuit [12]. The absorbance computations used Beer' and thus neglected the possible laser line broadening effects due to thermal frequency chirp [12]. The computation also used the pressure broadening coefficient for SO_2 in air contained in the HITRAN data base and thus neglects possible additional broadening due to collisions with H_2O and CO_2. Despite these limitations, the HITRAN and HITEMP spectral modeling computations provide the best estimates within the known state of the art for high-temperature, high-resolution infrared absorption by SO_2, H_2O, and CO_2.

However, the absorbance spectra for SO_2 (ʋ3), H_2O, and CO_2 in the 1321 to 1390 cm region (7.3 to 7.5 µm), for P = 1 atm, T = 700 K, ΩH_2O = 0.2, ΩCO_2 = 0.1, ΩSO_2 = 1 ppmv, were simulated [1]. The SO_2 absorbencies generally exceed those of CO_2, and are well above the estimated absorbance detection limit of ≈ 10^{-5}. Though, they are much lower than those of H_2O. Most significantly, at 1 atm the pressure-broadened wings of the H_2O transitions fill in the gaps between the evolutions, so that the H_2O absorbance is near-continuum which is always at least 100 times greater than that of SO_2 at 1 ppmv. Higher resolution simulations of selected gap in the H_2O spectrum indicate that spectral discrimination of SO_2 features under these conditions would be extremely difficult, and would require refined data processing and spectral fitting procedures to identify 10 to 100 ppmv of SO_2.

In distinction, there is a lot less H_2O interference in the $\upsilon1$ band, as shown in Figure 9 for the same 1 atm conditions. This is steady with our experimental observations at room temperature. Though the SO_2 absorbencies for 1 ppmv-m are near the probable detection limit of $\sim 10^{-5}$, the features of SO_2 are much easier to distinguish from the H_2O background in the spectral windows.
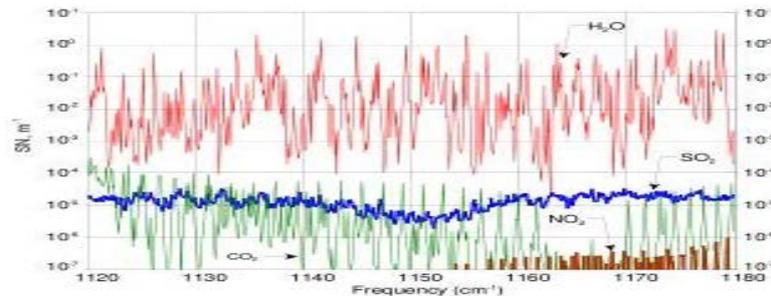
Figure 9: Computed atmospheric pressure exhaust gas absorption spectra near SO_2 (v1) band

Therefore at 1 atm and elevated temperature, SO_2 is probable to be further simply detected in the weaker $\upsilon1$ band than in the $\upsilon3$ band. Pro $\upsilon3$ band evolution at reduced pressure; the peak SO_2 absorbance for 1 ppmv-m is abridged, however yet surpass 10^{-5}. More importantly, the collision-broadened wings of the H_2O lines are seriously diminished, opening several spectral windows where SO_2 skin can be known. As abridged pressure conditions are more relevant to engine exit conditions at altitude, we focus on those conditions for more detailed computation in the SO_2 ($\upsilon3$) band.

To reproduce the conditions of engine exhaust measurements at high-altitude cruise conditions, we carry out a series of high-resolution calculations throughout the 1321 to 1390 cm region for P = 0.2 atm, T = 700 K, ΩH_2O = 0.1, ΩCO_2 = 0.1, ΩSO_2 = 1 ppmv. These calculations led to the recognition of three suitable spectral regions for detection of SO_2. These are illustrated in Figures 10 through 12. Here we show the entity contributions from H_2O, CO_2, and SO_2, and the sum of the three. In each of these spectral windows, a scan of the laser frequency will give quantitative identification of H_2O and SO_2; in addition, spectral scans near 1342 cm will give CO_2 determination as well. Gradual determinations of SO_2 along with H_2O and or CO_2 will allow direct determination of the emission index of SO_2 with a single sensor. The 1333 cm^{-1} region offers the strongest SO_2 evolution however the 1342 cm^{-1} region has better isolation of the SO_2 lines. The forecasted SO_2 crest absorbance in these windows for 1 ppmv-m are moderately above the probable detection limit of $\sim 10^{-5}$, which shows that sub-ppmv levels of SO_2 will probably be visible with a $\approx$ 1 m path length.
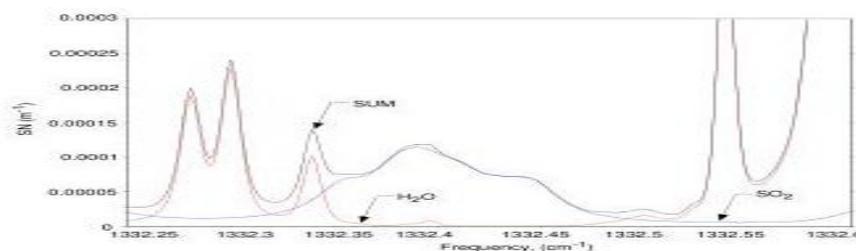
Figure 10: Computed exhaust gas spectra at 0.2 atm near 1332cm^{-1} (Courtesy Atmos.)
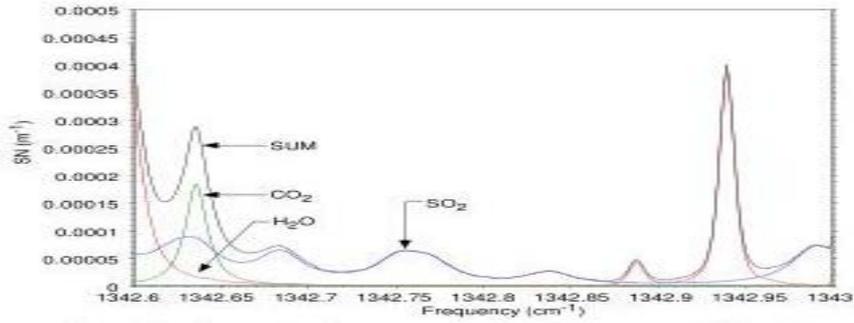
Figure 11: Computed exhaust gas spectra at 0.2 atm near 1343 cm^{-1} (Courtesy Atmos.)
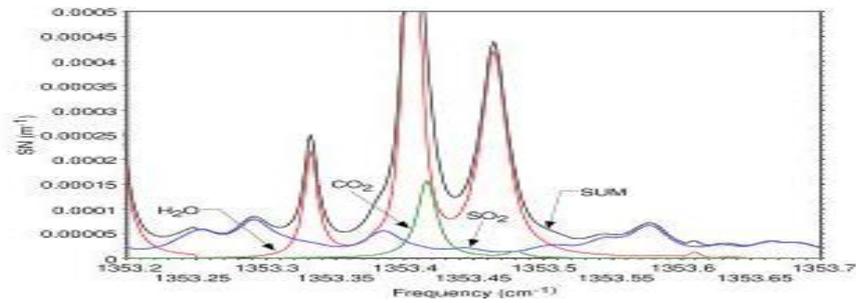
Figure 12: Computed exhaust gas spectra at 0.2 atm near 1354 cm^{-1} (Courtesy Atmos.)

Spectral model of the H_2O and CO_2 absorbance near the SO_3 band center are shown in Figure 13 for the 0.2 atm exhaust conditions. The H_2O baseline absorbance is fairly higher in this region, (2 to 4) x 10^{-4}. Depended on the peak absorbance of SO_3 at room temperature for this region, we estimate peak SO_3 absorbance for 1 ppmv-m to be about 8 x 10^{-5} as indicated by the bar on the graph.
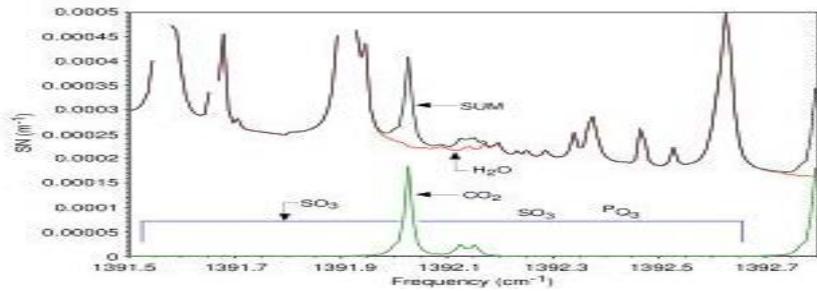
Figure 13: Computed exhaust gas spectra at 0.2 atm near 1392 cm^{-1} (Courtesy Atmos.)

SO_3 structure should be readily detectable among H_2O features near 1391.2 cm. It shows that SO_3 can likewise be detected to ~ 1 ppmv or less with a 1 m path length. Like with SO_2, it is likely that spectral scans of the laser will permit instantaneous determination of H_2O and/or CO_2, therefore docile the emission index of SO_3. There may be other spectral casement for detection of SO_3, nevertheless the region to lower frequency contains increasing contributions from SO_2 ($\upsilon3$), while the region to higher frequency contains increasing contributions from H_2O ($\upsilon2$). Decisive determination of the detection casement for SO_3 awaits direct spectral measurements at representative temperatures and pressures.

5. Conclusion

We used two mixtures of laboratory experimental measurements and spectral modeling calculation to evaluate and quantify the feasibility of high-sensitivity detection of SO_2 and SO_3 in combustor exhaust streams, using room-temperature quantum cascade laser absorption at precise operating wavelengths near 7 μm. Due to severe interference from collision broadened H_2O lines at 1 atm, it appears that the QC laser absorption method is best suited for the sub atmospheric conditions of high-altitude simulation test facilities when applied to the trace levels found in aircraft emission exhaust streams.

➢ **Spectral** modeling model of high-resolution infrared absorption spectra for high-altitude test chamber conditions (0.2 atm, 700 K) specify a few discrete spectral casement between 7 and 7.5 μm where SO_2 and SO_3 absorption features can be observed with minimal interference from H_2O and CO_2 in the exhaust stream. Through comparisons of the predicted peak absorbance and the expected detection limit given above, it is likely that both SO_2 and SO_3 can be detected at or below 1 ppmv, with a path length of 1 m, using a multipass optical system.

➢ **Laboratory** measurements of QC laser absorption by SO_2 at 8.6 μm shows a breadboard QC laser detection system and point to likely detection limits that can be achieved for a fully developed prototype sensor system. Based on straightforward projections of design improvements in laser intensity on detector, pulse generation electronics; heat-sinking of the laser chip, reduction of detector thermal noise, and quasi-cw balanced ratio metric rejection of common mode noise, we conservatively estimate a noise-equivalent absorbance detection limit of approximately $\approx 1 \times 10^{-5}$.

Acknowledgment

Reference

[1] Friedl, R.R. Atmospheric Effects of Subsonic Aircraft: Interim Assessment Report of the Advanced Subsonic Technology Program, NASA Reference Publication 1400, 1997.

[2] Wyslouzil, B.E., Carleton, K.L; Sonnenfroh, D.M; Rawlins, W.T; and S. Arnold, Observation of Hydration of Single, Modified Carbon Aerosols, Geophys. Res. Lett. 21, p. 2107, 1994

[3] Rawlins, W.T., Kang, S.G; Sonnenfroh, D.M; Carleton, K.L; and Wyslouzil, B.E; Activation of Carbon Aerosol by Deposition of Sulfuric Acid, Biomass Burning and Global Change, Levine, J.S; Edu MIT Press, Cambridge, MA, 1996, Vol. 1, pp. 540-544.

[4] Suto, M.; Ye, C; Ram, R.S; and Lee, L.C; SO_2 Fluorescence from Vacuum Ultraviolet Dissociative Excitation of SO_3, J. Phys. Chem. 91, p. 3262, 1987.

[5] Berkoff, T.A; Wormhoudt, J; and Miake-Lye, R.C; Measurement of SO_2 and SO_3 Using a Tunable Diode Laser System, SPIE Proceedings 3534, p. 686, 1998.

[6] Faist, J., Capasso, F; Sivco, D.L; Sirtori, C; Hutchinson, A.L; and Cho, A.Y; Science 264, p 553, 1994.

[7] Gmachl, C., Faist,J; Baillargeon, J.N; Capasso, F; Sartori, C; Sivco, D.L; et al Complex- Coupled Quantum Cascade Distributed-Feedback Laser, IEEE Photonics Tech. Letts. 9, p. 1090, 1997

[8] Namjou, K; Cai ,S; Whittaker, E.A; Faist, J; Gmachl, C; Capasso, F; et al Sensitive absorption spectroscopy with a room-temperature distributed-feedback quantum- cascade laser, Opt. Letts. 23, pp. 219-221, 1998

[9] Sharpe, S.W; Kelly, J.F; Hartman, J.S; Gmachl, C; Capasso, F; Sivco, D.L; et al High resolution Doppler limited spectroscopy using quantum- cascade distributed-feedback lasers, Opt. Letts. 23, pp. 1396-1398, 1998

[10] Paldus, B.A; Spence, T.G; Zare, R.N; Oomens, J; Harren ,F.J.M; Parker, D.H; et al Photoacoustic spectroscopy using quantum-cascade lasers, Opt. Letts. 24, pp. 178- 180, 1999.

[11] Kosterev, A.A., Curl, R.F; Tittel, F.K; Gmachl, C; Capasso, F; Sivco, D.L; et al Methane concentration and isotopic composition measurements with a mid-infrared quantum-cascade laser, Opt. Letts. 24, pp. 1762-1764, 1999.

[12] Sonnenfroh, D.M., Wetjen, E.W., Miller, M.F., Allen, M.G., Gmachl, C., Capasso, F., et al Mid-IR Gas Sensors Based on Quasi-CW, Room-Temperature Quantum Cascade Lasers, Paper No. 2000- 0641, 38th AIAA Aerospace Sciences Meeting, January, 2000. A revised version, Application of Balanced Detection to Absorption Measurements of Trace Gases with Room-Temperature, Quasi-CW QC Lasers, publication in Applied Optics, September, 2000.

[13] Allen, M.G., Carleton, K.L; Davis, S.J; Kessler, W.J; Otis, C.E; Palombo, D.A; et al Ultra-Sensitive Dual-Beam Absorption and Gain Spectroscopy: Applications for Near-IR and Visible Diode Laser Sensors, Appl. Opt. 34, p. 3240, 1995.

[14] Henfrey, N.S., and Thrush, B.A; The v3 Band of SO_3 at High Resolution, Chem. Phys. Lett. 102, p. 135, 1983.

[15] Oritgoso, J. R; Escribano, and A.G. Maki, The v2 v4 IR Bands of SO3, J. Mol Spectrosc. 138, p. 602, 1989.